The Visual Computer

Photorealistic image synthesis for outdoor scenery under various atmospheric conditions

Kazufumi Kaneda[1], Takashi Okamoto[2], Eihachiro Nakamae[1], and Tomoyuki Nishita[3]

[1] Faculty of Engineering, Hiroshima University, 4-1, Kagamiyama 1 chome, Higashi-hiroshima, 724 Japan
[2] Daikin Industry, Umeda Center Building, 2-4-12, Nishi-nakazaki, Kita-ku, Osaka, 530 Japan
[3] Faculty of Engineering, Fukuyama University, Higashimura-cho, Fukuyama, 729-02 Japan

We propose a method for displaying photorealistic images of outdoor scenes suitable for displaying simulation results, such as the appearance of a building under various weather conditions. This method portrays the changes in perceived color of buildings under various atmospheric conditions by taking into account the spectral distribution of both direct sunlight and sky light. Such views of buildings (including the effects of atmospheric particles like clouds, fog, and light beams) are useful for the design not only of buildings, but also of whole city areas.

Key words: Sky light – Specular reflection – Atmospheric scattering model – Fog effect – Spectral distribution

Offprint requests to: E. Nakamae

1 Introduction

There are two approaches for rendering images. One is to display realistic images for entertainment and art. The other is to display simulation results for visual environmental assessment and building design. In this paper, we take the latter approach.

Buildings have their own attributes, such as color and reflection. However, when the buildings are lit by sunlight under various atmospheric conditions, the hue of the buildings and their brightness and saturation change greatly. This is caused by various influences, such as the spectral distribution and intensity of light sources, which are determined by the position of the sun, atmospheric conditions, and the relationship between the position of the building and the various objects obscuring it. Considering these effects, for designing and pre-evaluating a building, it is particularly important to display not only the shape of the completed building but also its appearance, including the surroundings under various atmospheric conditions.

We propose a method for displaying photorealistic images of three-dimensional objects, such as buildings, and particles in the atmoshere, i.e., clouds, fog, and haze under various atmospheric conditions taking into account the spectral distribution of direct sunlight and sky light as an ambient light source.

2 Previous work

In order to simulate lighting effects for visual environmental assessment, both direct light and ambient light should be taken into account. So far, the following methods have been developed for this purpose.

For direct light, in the 1970s, a parallel light source was usually used. In the 1980s, methods for shading and shadowing three-dimensional objects lit by various artificial light sources, such as a point light source (Nishita et al. 1985a), linear light source (Nishita et al. 1985a), and area light source (Nishita and Nakamae 1983), were developed. Klassen (1987) proposed a method for displaying the color of the sun and the hue of the sky taking into account both scattering and absorption of the sunlight due to air molecules and aerosols in the atmosphere. Inakage (1989) improved Klassen's method by approximating geometric optics for large particles, such as raindrops. However, these methods are inadequate for generating realistic images for

The Visual Computer (1991) 7:247–258

visual assessment, because they do not take into account sky light and specular reflection.

For ambient light, in the 1970s, the method of adding either a uniform ambient light to the lighting model or a secondary light source coincident with the viewpoint was employed (Foly and van Dam 1982). In order to calculate the ambient light inside a room exactly, Cohen and Greenberg (1985) and Nishita and Nakamae (1985b) proposed a method for modeling the inter-reflection of light (radiosity). Using uniform ambient light, the phenomenon of color bleeding can be rendered, i.e., not only brightness but also hue and saturation of color are taken into account. Immel et al. (1986) and Kajiya (1986) developed a method considering specular reflection. Rushmeier and Torrance (1987) generalized the radiosity method for displaying beams of light due to particles in the atmosphere in a room. On the other hand, for ambient light in the open air, Nishita and Nakamae (1986) proposed a method for shading and shadowing taking sky light into account. This method, however, can only display the brightness under various weather conditions, without the effects on the hue and saturation of color caused by the spectral distribution of sky light. In other words, white was used for both direct sunlight and sky light, and the color of the sky was not modeled scientifically.

In order to render fog effects caused by the interaction between light and particles distributed in the three-dimensional space, Blinn (1982) developed a single scattering cloud model and displayed Saturn's rings consisting of reflective ice particles. However, the method is restricted to applying particles with a uniform distribution and a low albedo. He also described the necessity of developing a multiple scattering model with shadow effects in order to simulate various phenomena. Kajiya (1984) developed a multiple scattering model, in which particle densities are specified at three-dimensional grid points. He also rendered particles with high albedos, such as clouds. However, the calculation cost of the method is very expensive. Max (1986a) proposed a method for rapid calculation of atmospheric scattering due to particles with a uniform distribution and taking into account single reflection, by approximating exponential functions. Furthermore, by sorting the shadow edges using polar coordinates for efficiency, he displayed sunbeams shining through a break in the clouds or branches of trees (Max 1986b). Nishita et al. (1987) proposed an atmospheric scattering model taking into account luminous intensity distributions of light sources. He also introduced the idea of illumination volume for efficient calculation. However, these methods took no account of the effects of sky light.

Here, a method for creating photorealistic images of outdoor scenery, such as buildings and streets, taking into account specular reflection is proposed. In our proposed method, based on Klassen's model, the colors of the sun and sky (calculated by using an improved atmospheric scattering model) are employed for direct sunlight and sky light. Ways of displaying not only shading and shadowing, but also beam and fog effects caused by the direct sunlight and sky light with spectral distributions are described. By using the proposed method, outdoor images taking into account hue, brightness, and saturation can be created.

In the following sections, creating density distributions of particles in the atmosphere, rendering three-dimensional objects lit by direct sunlight and sky light, displaying beam and fog effects, and rendering clouds are discussed. Finally, some examples demonstrate the effectiveness of the method proposed.

3 Density distributions of particles in the atmosphere

3.1 Atmospheric scattering model

It is well known that sunlight is scattered or absorbed by the ozone layer, air molecules, and aerosols. For visible wavelengths of light, however, absorption in the ozone layer is negligible compared with absorption by air molecules and aerosols. For much smaller particles compared with the wavelength of the light, i.e., air molecules, Rayleigh scattering predominates. On the other hand, for particles with almost the same diameter as the wavelength of the light, i.e., aerosols, Mie scattering predominates.

Klassen's atmospheric scattering model divides the distribution of Rayleigh particles into two layers with uniformly distributed particles in each layer. However, in fact, the density of air molecules decreases exponentially with altitude. Thus, in our atmospheric scattering model, the light reflected due to Rayleigh scattering is calculated taking into account the density ratio of air molecules to the

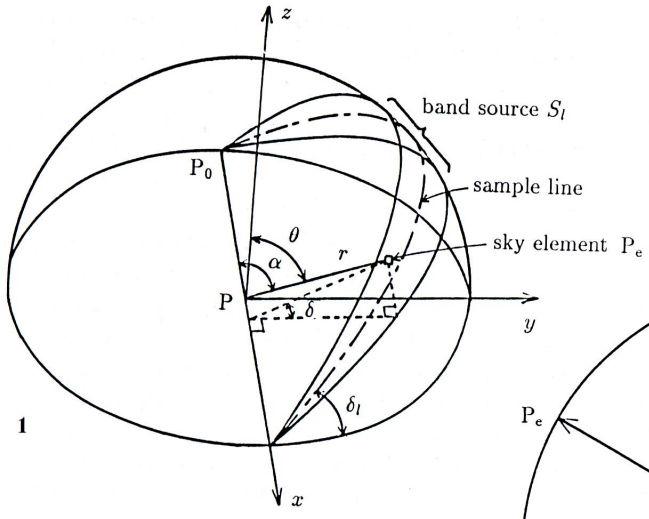

1

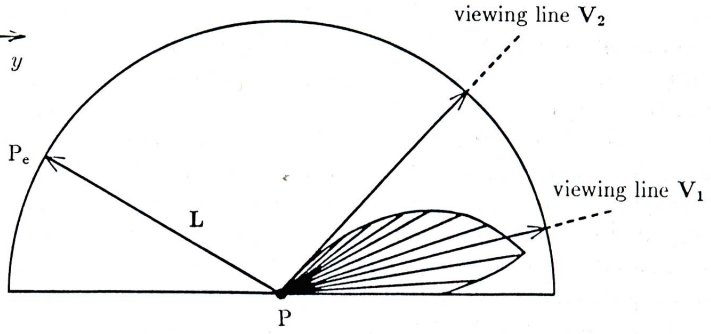

2

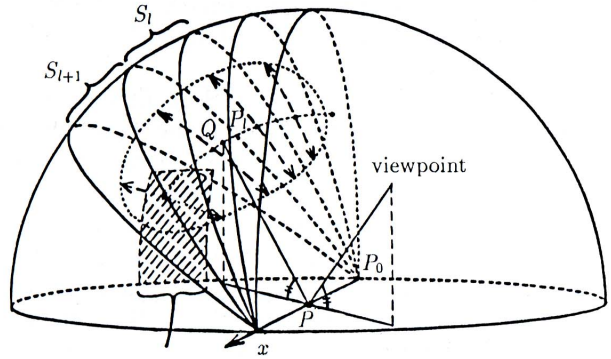

area obscured by an object

3

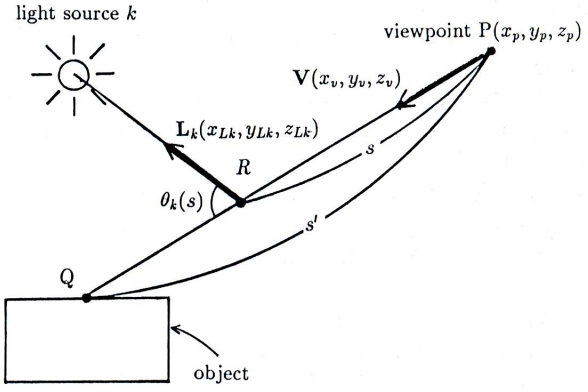

4

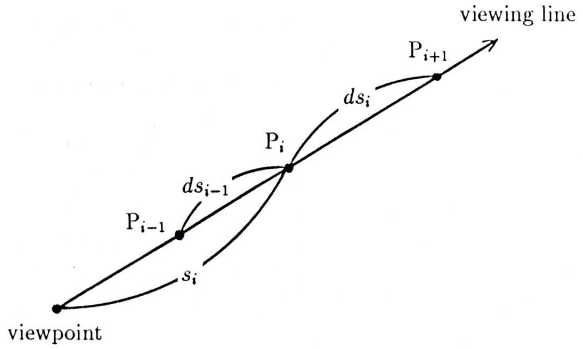

5

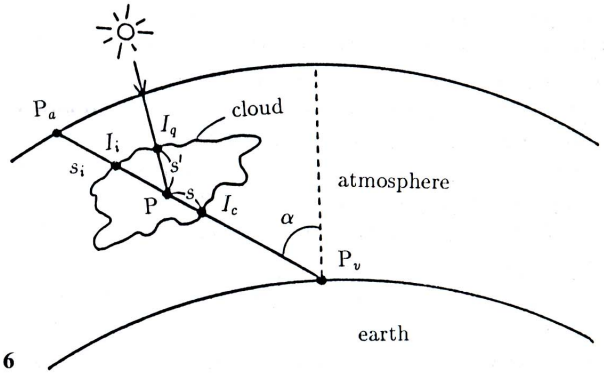

6

Fig. 1. Sky dome for calculation of sky light intensity (P = calculation point)

Fig. 2. Specular reflection due to the sky element

Fig. 3. Determination of the integral region for specular reflection due to sky light

Fig. 4. Calculation of beam and fog effects

Fig. 5. Numerical integration for displaying fog effect caused by sky light

Fig. 6. Scattering and absorption due to clouds

standard atmosphere (molecular density at sea level). The molecular density ratio ρ is given by

$$\rho = \exp\left(-\frac{h}{H_0}\right), \tag{1}$$

where h is the altitude above the sea level and H_0 is a scale height ($H_0 = 7994$[m]), which corresponds to the atmosphere thickness if the density were uniform.

In Klassen's model, the aerosols that cause Mie scattering are distributed in a flat layer. When the altitude of the sun is low, as in the case of dawn or sunset, the distance between the sun and the calculation point, passing through the atmosphere with aerosols, becomes infinite. To deal with this problem, the spherical-shell atmosphere used for the air molecules mentioned above is used in our atmospheric scattering model. From the view point of a macro-sized object like the earth, the density of aerosols decreases exponentially with altitude, just as the density distribution of air molecule does, even though the rate of decrease is different from that of air molecules. The density can be calculated by setting the scale height, H_0, of Eq.(1) to 1.2 km (Sekine 1987).

Displaying fog, in which the density has a different distribution from that mentioned above and is much higher, is described in the next paragraph.

3.2 Density distribution of fog

In order to render fog effects, whose densities vary with the altitude, the distribution of particles has been divided into several layers with uniformly distributed particles in each layer (Nishita et al. 1987). However, it is well known that the density of particles that cause a beam or fog, like the density of vapor and aerosols, decreases in an exponential or similar way. Therefore, the method in (Nishita et al. 1987) cannot be employed to render natural fog effects.

In the proposed method, the distribution of particles is approximated as an exponential function. If a unit vector from the viewpoint P (x_p, y_p, z_p) to the point Q is expressed by V (x_v, y_v, z_v), then the particle density at a point R is given by

$$\rho(s) = \rho_0 \cdot \exp\left(-\frac{z(s)}{h_0}\right), \tag{2}$$

where ρ_0 is the particle density at the altitude of zero meters, h_0 is a scale height for the particles, and $z(s) = z_p + z_v \cdot s$, where s is the distance between the points P and R (see Fig. 4).

4 Rendering 3-D objects lit by sky light

In this section, we discuss a method for rendering three-dimensional objects lit by sky light taking into account both diffuse and specular reflections. For the calculation of the spectral distribution of sky light, the atmospheric scattering model described in the previous section is employed.

The sky is taken as a hemisphere light source with a large radius (called the sky dome, see Fig. 1), and the dome is subdivided into several band sources in the same way as those of Nishita and Nakamae (1986). It is assumed that in each band source, the intensity of light varies in the band axis direction and is fixed at a constant value in the width direction.

In the case of the diffuse reflection described in Nishita and Nakamae (1986), the band width is allowed to be fairly wide and is fixed due to the constant intensity of diffuse reflection in every direction. On the other hand, it is well known that the intensity of specular reflection tends to the specified direction. Therefore, in this case, a part of the sky dome may be enough for the calculation of specular reflection, even though the band width is narrow.

4.1 Specular reflection due to sky light

In this paper, the Cook-Torrance model (1982) is employed for calculating specular reflection due to sky light, because of its ability to generate high-fidelity images and the fact that it takes into account the spectral distribution.

It is assumed that a sky element P_e consisting of a band source is treated as a point-light source, and the position of P_e is defined by two angles; i.e., the angle α from the x-axis to the sky element and the angle δ from the horizontal plane to the sky element (Fig. 1). By adding the effect of the specular reflection to Eq.(1) (Nishita and Nakamae 1986), the intensity of the specular reflection at the calculation point P due to the sky element is given by:

$$dI = R_s(\alpha, \delta, \mathbf{V}) \cdot L(\alpha, \delta) \cdot \sin\alpha \cdot \sin\delta \cdot r^{-2} \cdot dA, \tag{3}$$

where $R_s(\alpha, \delta, \mathbf{V})$ is the specular reflectance, $\mathbf{V}$ is the unit vector from the calculation point P toward the viewpoint, $L(\alpha, \delta)$ is the intensity of the sky element, r is the distance of $\overline{PP_e}$, and dA is the area of the sky element and is given by

$$dA = (r \cdot d\alpha) \cdot (r \cdot d\delta \cdot \sin \cdot \cdot \alpha). \tag{4}$$

By integrating Eq.(3), the intensity of the specular reflectance due to the band source S_l is obtained as

$$I_l = \int_0^{\pi} \int_{\delta_l - \Delta_l}^{\delta_l + \Delta_l} R_s(\alpha, \delta, \mathbf{V}) \cdot L(\alpha, \delta) \cdot \sin \delta \cdot \sin^2 \alpha \cdot d\delta \cdot d\alpha. \tag{5}$$

In such a narrow band as defined above ($\delta_l - \Delta_l \leqq \delta \leqq \delta_l + \Delta_l$) where $2\Delta_l$ is the angular width of a band source, both the intensity of the sky element and the specular reflectance can be held constant. Then $L(\alpha, \delta)$ and $R_s(\alpha, \delta, \mathbf{V})$ are expressed by $L(\alpha, \delta_l)$ and $R_s(\alpha, \delta_l, \mathbf{V})$, respectively. In this paper, the angle δ is sampled as $\cos(\delta_l - \Delta_l) - \cos(\delta_l + \Delta_l) = 1/N$ (constant), where N is the number of the band sources. Thus, Eq.(5) becomes

$$I_l = \frac{1}{N} \cdot \int_0^{\pi} R_s(\alpha, \delta_l, \mathbf{V}) \cdot L(\alpha, \delta_l) \cdot \sin^2 \alpha \cdot d\alpha. \tag{6}$$

Then, the intensity of the specular reflection due to the sky dome is given by

$$I = \sum_{l=1}^{N} I_l. \tag{7}$$

4.2 Calculation of specular reflection

For a rapid calculation of specular reflection due to sky light, it is almost impossible to obtain look-up tables like those for the intensity of the diffuse reflection, because the specular reflectance depends on the viewpoint. Using one property of specular reflectance, however, may save calculation time. If the direction of regular reflection to the sky element P_e is almost coincident with the direction of the viewing line, the specular reflectance toward the viewing line is extremely large, while if not, much less intensity of specular reflection due to the sky element arrives at the viewpoint (Fig. 2). These facts suggest that the intensity of specular reflection due to the sky dome can be calculated without any compensation for preciseness by integrating a part of the sky dome in Eq.(7), that is, with an appropriate integral width and range.

It is assumed that the function G for determining the integral range is defined as

$$G(\alpha, \delta, \mathbf{V}) = L(\alpha, \delta) \cdot R_s(\alpha, \delta, \mathbf{V}) \cdot \sin \alpha. \tag{8}$$

If the threshold value is ε, then the integral range is limited to the regions where $G(\alpha, \delta, \mathbf{V})$ is greater than ε. The integral area cannot be determined a priori, because the function depends not only upon the specular reflectance, but also on obstacles casting shadows. In the proposed method, the integral starts from a location where the function has a large value and proceeds to a small value area, that is, from the sky element in the direction of the regular reflection to away from the sky element. The algorithm of the integration is as follows (Fig. 3):

1) Obtain the point Q where the direction of the regular reflection for the viewing line intersects with the sky dome. It is assumed that the point Q is located between two sample lines of the band sources S_l and S_{l+1}, where a sample line is defined by the center line of the band source (Fig. 1). Then the tilt angle δ_l of the sample plane, which is defined as the plane including the sample line of the band source S_l and x-axis is calculated (Fig. 1).

2) Search for the sky element P_l, which is closest to the point Q along the sample line of the band source S_l, and calculate the angle α_{l1} between x-axis (PP_0) and PP_l. If $G(\alpha_{l1}, \delta_l, \mathbf{V}) \geqq \varepsilon$, then integrate over the band source S_l as follows:

(a) Execute trapezoidal integration along the sample line from the sky element $P_l(\alpha_{l1}, \delta_l)$ toward one of the end of the line with a pitch $d\alpha$ corresponding to the width of a segment, until the condition $G(\alpha_{l1}, \delta_l, \mathbf{V}) < \varepsilon$ is satisfied. When a segment of the sample line is obscured by obstacles, the integral of that segment is skipped. The visible segments are obtained by calculating the intersections of the sample plane and the obstacles.

(b) Integrate the sample line from the sky element $P_l(\alpha_{l1}, \delta_l)$ toward the other end of the line in the same way as explained in (a).

3) For an adjacent band source S_{l-1}, process (2) is employed when $G(\alpha_{l1}, \delta_l, \mathbf{V}) > \varepsilon$ at the border of S_l.

4) Continue the above-mentioned process for the band sources S_{l-2}, S_{l-3} and so on. If the condition

$G(a_{i1}, \delta_i, \mathbf{V}) < \varepsilon$ is satisfied at P_i, which is the closest sample segment to the point Q on the sample line of the band source $S_i (i = l-1, l-2, \ldots, 1)$, then the integration is stopped.

5) For the other side of the band sources S_{l+1}, $S_{l+2}, \ldots, S_i, \ldots, S_N$, the processes from (2) to (4) are employed until the condition, $G(\alpha_{i1}, \delta_i, \mathbf{V}) < \varepsilon$ is satisfied.

5 Rendering beam and fog effects

Due to vapor and particles in the atmosphere, the path of the light brightens and the intensity of the light weakens before arriving at the viewpoint. A method for rendering beam and fog effects caused by direct sunlight and sky light is discussed in this section. The spectral distributions of direct sunlight and sky light are also calculated by using the atmospheric scattering model.

The attenuation coefficient, scattering ratio of light while passing through a distance unit in the atmosphere, is proportional to the particle density and is given by

$$\tau(s) = \rho(s) \cdot \tau_0 \cdot \left(\frac{\lambda}{\lambda_0}\right)^{-b}, \tag{9}$$

where $\rho(s)$ is the particle density specified by Eq.(2), λ is the wave length of incident light, λ_0 is a standard wavelength, τ_0 represents the scattering coefficient of the standard wavelength with unit particle density, and b is a coefficient determined by particle size of fog. Then, the optical length $t(s)$ from the viewpoint P to the point R (Fig. 4) is obtained by

$$t(s) = \int_0^s \tau(s) \cdot ds. \tag{10}$$

If the distance between P and Q is s' and the intensity of the surface at Q is I_0, the intensity of the ray arriving at the viewpoint P is given by

$$I = I_0 \cdot \exp(-t(s')) + \sum_k \cdot \int_0^{s'} \tau(s) \cdot J_k(s) \cdot \exp(-t(s)) \cdot ds, \tag{11}$$

where $J_k(s)$ is the light function of the light source k at the viewpoint P and is given by

$$J_k(s) = I_k(s) \cdot \exp(-t'_k(s)) \cdot F(\theta_k(s)), \tag{12}$$

where $I_k(s)$ represents the intensity of the ray arriving at point R under the condition of no particles and is calculated by using direct sunlight and sky light, which are obtained by the atmospheric scattering model, $t'_k(s)$ is an optical distance between the light source k and the point R, and $F(\theta_k(s))$ is a phase function.

In order to display light beams taking into account obstacles, the integration is performed only for visible sections of light on the viewing line, where the section is obtained by using shadow volumes (Crow 1977). Integration in the cases of direct sunlight and sky light is described below.

5.1 Direct sunlight

As the direct sunlight is a parallel light source, $\theta_k(s)$ becomes constant. Then, Eq.(11) can be calculated analytically (see Appendix), because $F(\theta_k(s))$ in Eq.(12) has a constant value.

5.2 Sky light

Sunbeams often appear when direct sunlight with high intensity passes through particles in the atmosphere. On the other hand, when a fog or a mist is lit by sky light, the whole atmosphere is brightened. In the latter case, numerical integration must be employed for calculating Eq.(11), because the analytical integration used for a parallel light source (direct sunlight) cannot be employed. For simplifying the calculation, in this case, we assume the conditions of a uniform phase function and no shadow effects of obstacles.

The intensity of sky light $J_k(s)$ arriving at the point P_i (Fig. 5) is obtained by integrating the sky elements along all band sources:

$$J_k(s_i) = \sum_{i=1}^{N} W_l \cdot \int_0^{\pi} L(\alpha, \delta) \cdot \sin\alpha \cdot \exp(-t'(s_i)) \cdot d\alpha, \tag{13}$$

where N is the number of the band sources, W_l is the angular width of the band source l, $L(\alpha, \delta)$ is the intensity of the sky element, and $t'(s_i)$ is an optical distance btween the point P_i and each sky element.

By introducing the two assumptions described above, $J_k(s_i)$ can be expressed by a function of the altitude of P_i only. In other words, the light function is independent from of the x and y coordinates

of the point P_i and the directions of viewing line and ray. Therefore, look-up tables of $J_k(s_i)$ at every altitude can be created in advance.

In order to calculate the intensity of the scattered light along the viewing line, trapezoidal integration is employed. That is, the integral starts from the viewpoint with a pitch, ds_i, which is determined by using (Fig. 5)

$$ds_i = \max\left(ds_{min}, \min\left(ds_{max}, \frac{ds_0}{\tau(s_i)\cdot J_k(s_i)\cdot\exp(-t(s_i))}\right)\right), \tag{4}$$

where ds_{min} and ds_{max} are the minimum and maximum pitches, respectively, and ds_0 is a standard pitch. The integration is continued until the condition $\tau(s_i)\cdot J_k(s_i)\cdot\exp(-t(s_i)) < \varepsilon$ is satisfied.

6 Rendering clouds

The size of particles in clouds is larger than that of air molecules or of aerosols mentioned before. Light scattered by large particles, such as those in clouds (Fig. 6), is little influenced by wavelength. However, the spectral distribution of the sunlight onto clouds depends to a fair degree on the position of the sun. The light passing through a cloud should be determined by three components: (i) sky light attenuated by passing through the cloud, (ii) light scattered and absorbed by cloud particles illuminated by direct sunlight, and (iii) ambient light caused by multiple scattering due to cloud particles.

For calculating the first component, the intensity of sky light on the cloud surface I_i is obtained by using the above-mentioned atmospheric scattering model. For the second component, the intensity of direct sunlight I_q is assumed to be constant everywhere on the face of a cloud, because the cloud thickness is much smaller than that of the atmosphere. Therefore, when the distance between the cloud center and the top of the atmosphere is Q, the intensity of direct sunlight on the cloud surface is given by

$$I_q = I_s(\lambda)\exp(-t(Q,\lambda)). \tag{15}$$

where $I_s(\lambda)$ is the solar radiation at the top of the atmosphere and $t(Q, \lambda)$ is the optical length of the distance Q for the wavelength λ. For the third component, ambient light due to cloud particles is assumed to have uniform intensity for all directions.

Finally, the intensity of light just after passing through the cloud I_c, taking into account the three components mentioned above, is obtained by (Fig. 6)

$$I_c(\lambda) = I_i(\lambda)\cdot\exp(-t(s_i)) + \int_0^{s_i} (I_q(\lambda)\cdot F(\theta) + I_a) \cdot\exp(-t(s)-t(s'))\cdot\rho_c(s)\cdot ds, \tag{16}$$

where I_a is the ambient light and both the phase function F and the density of the cloud ρ_c are assumed to be uniform. The shape of the cloud is defined by mapping a thickness function [Fourier series composed of a polynomial of sine waves (Gardner 1985)] onto an ellipse.

7 Examples

Figure 7 shows a building design application. The walls of the building in Fig. 7a–c are made of tiles (which have mainly diffused reflection), and the material in Fig. 7d–f is aluminum (which has practically only specular reflection). Figure 7a and d is in the morning (solar altitude is 17°), Fig. 7b and e, at noon (60°), and Fig. 7c and f, at sunset (4°). These examples demonstrate the variation in the hue and brightness of the building and the sky color. Figure 7a–c shows the variation of the building's hue due to the sun's position. Even though the actual color varies, as shown in these examples, human eyes usually don't perceive such large differences in the hue on the walls. Human visual perception takes into account expectations of color and color difference of various objects in the environment rather than their absolute spectral distribution. As a result, people do not usually notice this type of color shift. Figure 7a–d shows the color of the highlight on the building is mainly influenced by the specular reflection of the direct sunlight, and Fig. 7d–f shows that the hue of the building varies according to the sky light, except for the highlight region.

Figure 8 demonstrates how fog reacts to direct sunlight as well as to sky light and shows the variation in the appearance of the buildings. In Fig. 8a, the parameters ρ_0 and h_0 [in Eq.(2)] are set to 0.59 and 10.0, respectively, so the higher the altitude, the lower the density. On the contrary, in Fig. 8b,

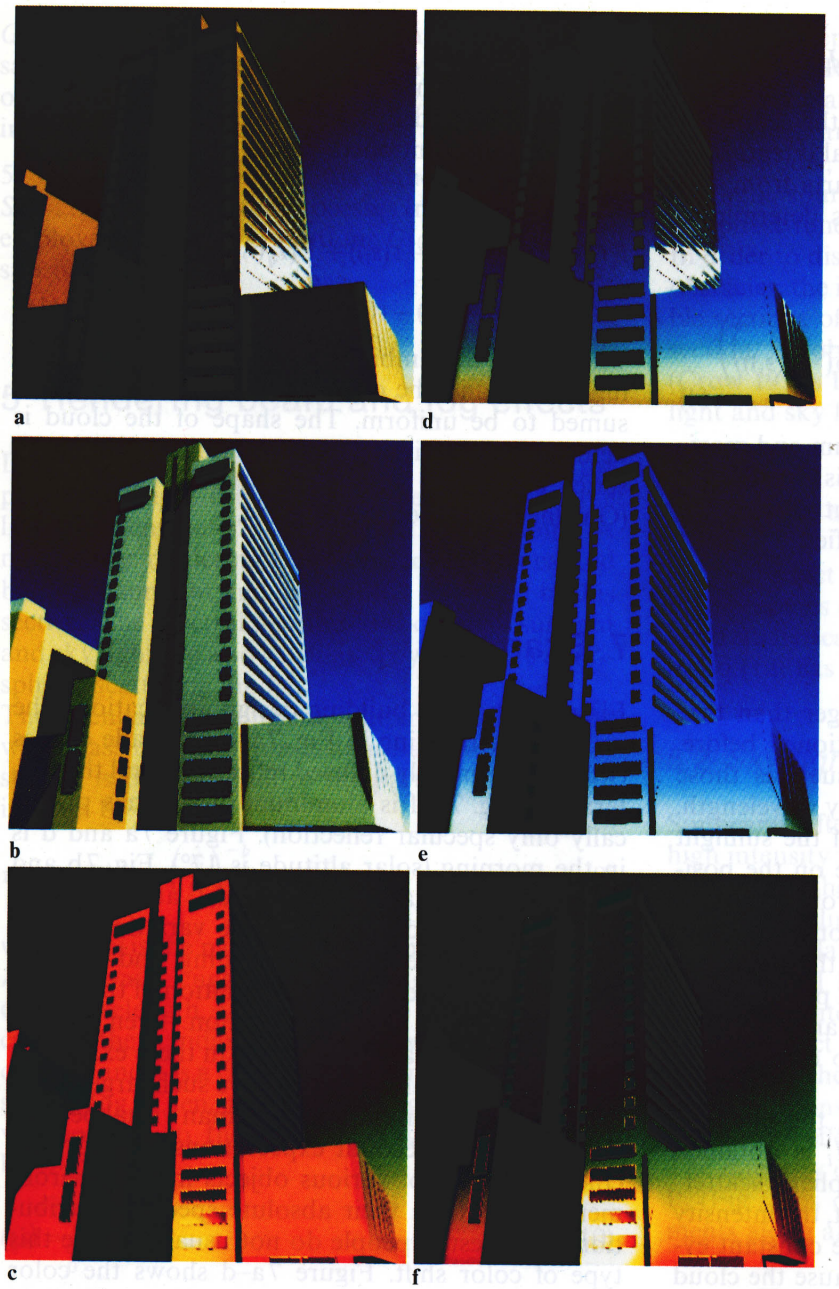

Fig. 7a–f. Examples of changing color of the building according to the solar altitude and the material of the walls

the parameters ρ_0 and h_0 are set to 0.037 and -15.0, respectively. Figure 8c, d displays silhouette and beam effects at different times; the position of the sun changes between these figures.

Figure 9 also shows the beam and fog effects in the night scene; the distributions of luminous intensities of automobile headlights and street lamps are also taken into account.

In Fig. 10a, the position of the sun is set in front of the building, while in Fig. 10b it is set behind the building. These examples demonstrate that when the sun is in front of the viewpoint, the edges of the clouds are brighter than their central area, because of their thickness, while when the sun is behind the viewpoint, the side of the clouds lit by direct sunlight is brighter than the other side.

Using IRIS-4D/70GT, it took about 20 h to calculate Fig. 8a and 17 h to calculate Fig. 10b.

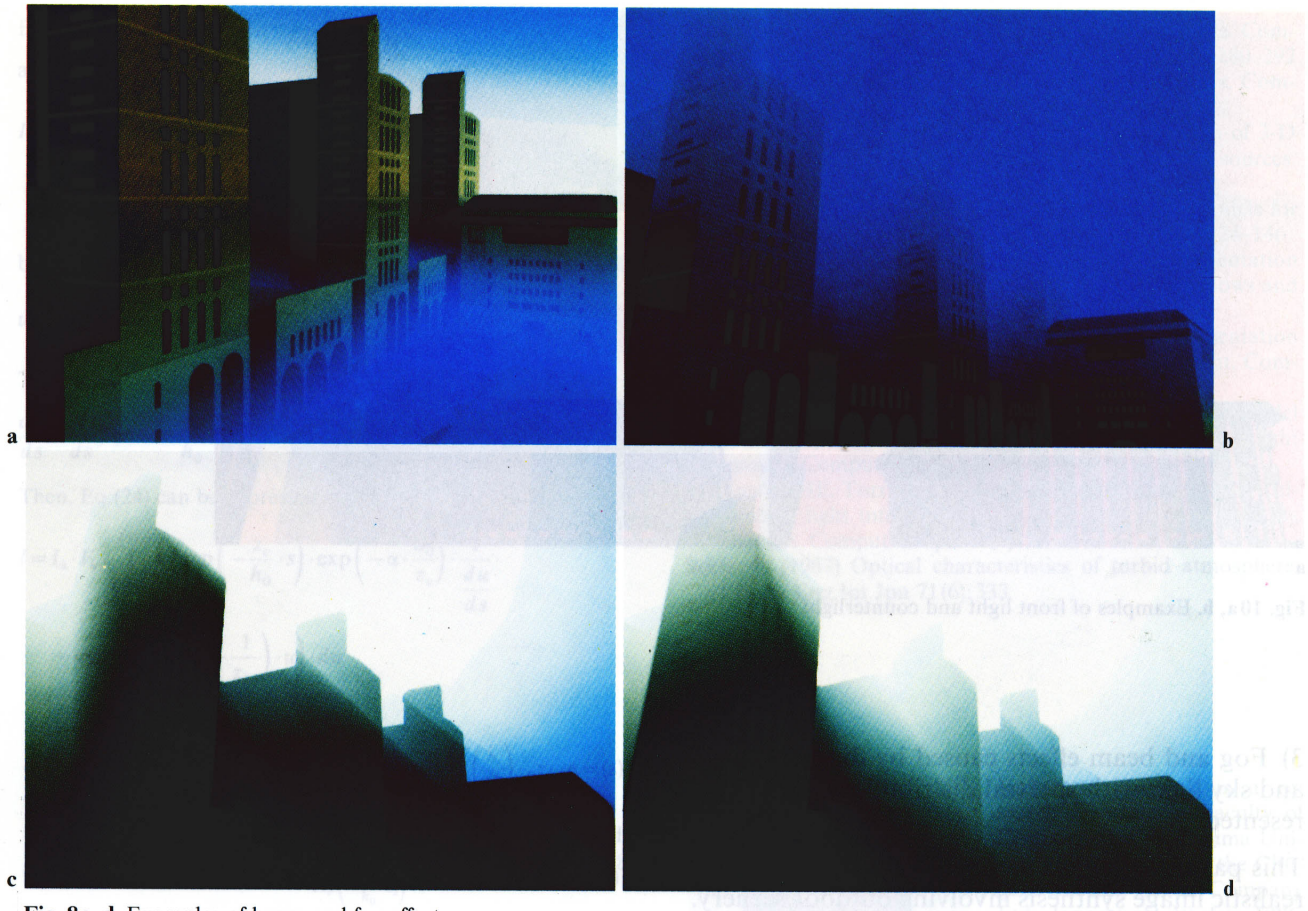

Fig. 8a–d. Examples of beam and fog effects

Fig. 9. Example of beam and fog effects in the night

8 Conclusions

Photorealistic image synthesis techniques of outdoor scenery are proposed from the view point of displaying the simulation results for designing buildings and performing assessments of their visual impact.

The proposed method has the following advantages:

1) The hues of the sky, clouds, and buildings vary according to both the position of the sun and atmospheric conditions.

2) Buildings lit by both direct sunlight and sky light can be rendered taking into account both diffuse and specular reflections.

a b

Fig. 10a, b. Examples of front light and counterlight

3) Fog and beam effects caused by direct sunlight and sky light with spectral distribution can be represented.

This paper developed an important part of photo-realistic image synthesis involving outdoor scenery. For rendering outdoor images under more varied conditions as accurately and quickly as possible, several further studies are needed. These include developing a high-speed rendering and a method for handling weather conditions, such as rain and snow.

Acknowledgment. The data were provided by the Osaka Municipal Government.

Appendix: Intensity of parallel light scattered by fog

We assume that fog is distributed in a flat layer, because it usually occurs in a local area.
The illuminance at the point R and $F(\theta_k(s))$ without fog is given by

$$I_k(s)=I_k, \tag{17}$$

$$F(\theta_k(s))=F_k, \tag{18}$$

where both I_k and F_k have a constant parallel-light value (Fig. 4). By integrating the attenuation coefficient between the point R and the light source (the distance is infinite), its optical distance $t'(s)$ is given by

$$t'(s)=\rho_0\cdot\tau_0\cdot\left(\frac{\lambda}{\lambda_0}\right)^{-b}\cdot\exp\left(-\frac{z_p+z_v\cdot s}{h_0}\right)\cdot\frac{h_0}{z_{Lk}}. \tag{19}$$

Then, the light function $J_k(s)$ is given by

$$J_k(s)=I_k\cdot F_k\cdot\exp(-t'(s)). \tag{20}$$

Intensity of light scattered by fog between s_1 and s_2 is given by

$$I=\int_{s_1}^{s_2}\tau(s)\cdot J_k(s)\cdot\exp(-t(s))\cdot ds. \tag{21}$$

To simplify this equation, the following substitution is introduced:

$$\alpha=\rho_0\cdot\tau_0\cdot\left(\frac{\lambda}{\lambda_0}\right)^{-b}\cdot\exp\left(-\frac{z_p}{h_0}\right). \tag{22}$$

Then, Eq.(21) is solved by:

1) for $z_v=0$,

$$I=I_k\cdot F_k\cdot\int_{s_1}^{s_2}\exp\left(-\alpha\cdot\frac{h_0}{z_{Lk}}\right)\cdot\alpha\cdot\exp(-\alpha\cdot s)\cdot ds$$

$$=I_k\cdot F_k\cdot\exp\left(-\alpha\cdot\frac{h_0}{z_{Lk}}\right)\cdot[\exp(-\alpha\cdot s)]_{s_2}^{s_1}. \tag{23}$$

(2) for $z_v\neq 0$,

$$I=I_k\cdot F_k\cdot\int_{s_1}^{s_2}\alpha\cdot\exp\left(-\frac{z_v}{h_0}\cdot s\right)\cdot\exp\left(-\alpha\cdot\frac{h_0}{z_v}\right)$$

$$\cdot\exp\left(\alpha\cdot h_0\cdot\left(\frac{1}{z_v}-\frac{1}{z_{Lk}}\right)\cdot\exp\left(-\frac{z_v}{h_0}\cdot s\right)\right)\cdot ds. \tag{24}$$

Eq. (24) is solved by:

a) for $z_v = z_{Lk}$,

$$I = I_k \cdot F_k \cdot \int_{s_1}^{s_2} \alpha \cdot \exp\left(-\alpha \cdot \frac{h_0}{z_v}\right) \cdot \exp\left(\frac{-z_v}{h_0} \cdot s\right) \cdot ds$$

$$= I_k \cdot F_k \cdot \alpha \cdot \exp\left(-\alpha \cdot \frac{h_0}{z_v}\right) \cdot \frac{h_0}{z_v} \cdot \left[\exp\left(-\frac{z_v}{h_0} \cdot s\right)\right]_{s_2}^{s_1}. \quad (25)$$

b) for $z_v \neq z_{Lk}$, we use the following integration by substitution:

$$u = f(s) = \exp\left(-\frac{z_v}{h_0} \cdot s\right). \quad (26)$$

Therefore,

$$\frac{du}{ds} = \frac{d}{ds} f(s) = -\frac{z_v}{h_0} \cdot \exp\left(-\frac{z_v}{h_0} \cdot s\right). \quad (27)$$

Then, Eq.(24) can be expressed by:

$$I = I_k \cdot F_k \cdot \int_{f(s_1)}^{f(s_2)} \alpha \cdot \exp\left(-\frac{z_v}{h_0} \cdot s\right) \cdot \exp\left(-\alpha \cdot \frac{h_0}{z_v}\right) \cdot \frac{1}{\frac{du}{ds}}$$

$$\cdot \exp\left(\alpha \cdot h_0 \cdot \left(\frac{1}{z_v} - \frac{1}{z_{Lk}}\right) \cdot u\right) \cdot du$$

$$= I_k \cdot F_k \cdot \frac{\exp\left(-\alpha \cdot \frac{h_0}{z_v}\right)}{1 - \frac{z_v}{z_{Lk}}}$$

$$\cdot \left[\exp\left(\alpha \cdot h_0 \cdot \left(\frac{1}{z_v} - \frac{1}{z_{Lk}}\right) \cdot u\right)\right]_{\exp\left(-\frac{z_v}{h_0} \cdot s_2\right)}^{\exp\left(-\frac{z_v}{h_0} \cdot s_1\right)}. \quad (28)$$

References

Blinn JF (1982) Light reflection functions for simulation of clouds and dusty surfaces. Comput Graph 16(3):21–29

Cohen MF, Greenberg DP (1985) A radiosity solution for complex environment. Comput Graph 19(3):31–40

Cook RL, Torrance KE (1982) A reflectance model for computer graphics. ACM Trans Graph 1(1):7–24

Crow FC (1977) Shadow algorithms for computer graphics. Comput Graph 11(2):242–247

Foley JD, van Dam (1982) Fundamentals of interactive computer graphics. Addison-Wesley

Gardner GY (1985) Visual simulation of cloud. Comput Graph 19(3):297–303

Immel DS, Cohen MF, Greenberg DP (1986) A radiosity method for non-diffuse environments. Comput Graph 20(4):133–142

Inakage M (1989) An illumination model for atmospheric environment. Proc CGI'89 pp 533–548

Kajiya JT (1984) Ray tracing volume densities. Comput Graph 18(3):165–174

Kajiya JT (1986) The rendering equation. Comput Graph 20(4):143–150

Klassen RV (1987) Modeling the effect of the atmosphere on light. ACM TRans Graph 6(3):215–237

Max NL (1986) Light diffusion through clouds and haze. Computer Vision, Graphics, and Image Processing 33(3):280–292

Max NL (1986) Atmospheric illumination and shadows. Comput Graph 20(4):117–124

Nishita T, Nakamae E (1983) Half-tone representation of 3-D objects illuminated by area sources or polyhedron sources. IEEE COMPSAC 83:237–242

Nishita T, Okamura I, Nakamae E (1985) Shading models for point and linear sources. ACM Trans Graph 4(2):124–146

Nishita T, Nakamae E (1985) Continuous tone representation of three-dimensional objects taking account of shadows and interreflection. Comput Graph 19(3):23–30

Nishita T, Nakamae E (1986) Continuous tone representation of three-dimensional objects illuminated by sky light. Comput Graph 20(4):125–132

Nishita T, Miyawaki Y, Nakamae E (1987) A shading model for atmospheric scattering considering distribution of light sources. Comput Graph 21(4):303–310

Rushmeier HE, Torrance KE (1987) The zonal method for calculating light intensities in the presence of a participating medium. Comput Graph 21(4):293–302

Sekine S (1987) Optical characteristics of turbid atmosphere. J Illum Eng Int Jpn 71(6):333

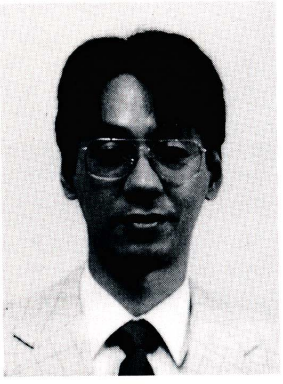

KAZUFUMI KANEDA is a research associate in Faculty of Engineering at Hiroshima University. He worked at the Chugoku Electric Power Company Ltd., Japan from 1984 to 1986. He joined Hiroshima University in 1986. His research interests include computer graphics and image processing. Kaneda received the BE, ME, and DE in 1982, 1984, and 1991, respectively, from Hiroshima University. He is a member of IEE of Japan, IPS of Japan and IEICE of Japan.

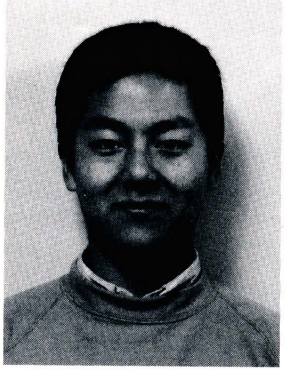

TAKASHI OKAMOTO is an engineer of Daikin Industry Ltd., which he joined in 1990. His research interests include computer graphics and its application. Okamoto received the BE and ME degrees in 1988 and 1990, respectively, from Hiroshima University. He is a member of IPS of Japan.

EIHACHIRO NAKAMAE is a professor at Hiroshima University where he was appointed as research associate in 1956 and a professor in 1968. He was an associate researcher at Clarkson College of Technology, Potsdam, N.Y., from 1973 to 1974. His research interests include computer graphics and electric machinery. Nakamae received the BE, ME, and DE degrees in 1954, 1956, and 1967 from Waseda University. He is a member of ACM, IEEE, IEE of Japan, IPS of Japan and IEICE of Japan.

TOMOYUKI NISHITA is a professor in the department of Electronic and Electrical Engineering at Fukuyama University, Japan. He was on the research staff at Mazda from 1973 to 1979 and worked on design and development of a computer-controlled vehicle system. He joined Fukuyama University in 1979. He was an associate researcher in the Engineering Computer Graphics Laboratory at Brigham Young University Utah, from 1988 to the end of March, 1989. His research interests involve computer graphics including lighting models, hidden-surface removal, and antialiasing. Nishita received his BE, ME and Ph. D in Engineering in 1971, 1973, and 1985, respectively, from Hiroshima University. He is a member of ACM, IPS of Japan, IEICE of Japan and IEE of Japan.